Development of a Finite Element Model of the Achilles Tendon

Evaluating Local Displacement Estimation

Master's Thesis

R.D. Beinema

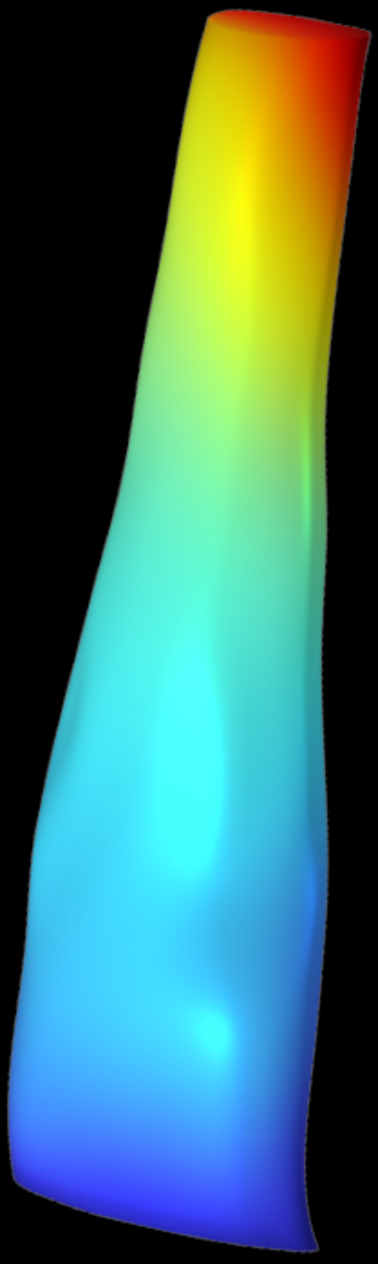

Delft University of Technology

TU Delft

Development of a Finite Element Model of the Achilles Tendon

Evaluating Local Displacement Estimation

by

R.D. Beinema

(4714105)

Instructors:	Dr. ir. E. van der Kruk
	Dr. ir. N. Tümer
	Dr. R.J. de Vos
Committee Members:	Dr. ir. E. van der Kruk
	Dr. ir. N. Tümer
	Dr. ir. F.J.H. Gijsen
Institution:	Delft University of Technology
Faculty:	Faculty of Mechanical Engineering (ME), Delft
Laboratory:	Biomechanical Optimization of Daily life, Exercise & Sports (BODIES)
Degree:	Master of Science in Mechanical Engineering
Presentation and Defense:	8 Apr 2024, 9:00 - 11:00

TU Delft

Development of a Finite Element Model of the Achilles Tendon: Evaluating Local Displacement Estimation

Rimke Beinema (4714105)

Faculty of Mechanical Engineering - Department of BioMechanical Engineering,
Delft University of Technology, Delft, The Netherlands
Supervisors: Eline van der Kruk, Nazli Tümer, Robert-Jan de Vos
Master Thesis BioMechanical Design - April 8 2024

***Abstract*— Achilles tendinopathy (AT) is a common Achilles tendon injury, yet its exact cause and the factors influencing progression of individuals remain unclear. Strain distribution is indicated to play a significant role in the progression, possibly linked to the twist of the subtendons. Pizzolato et al. (2020) proposed an integrated framework for studying Achilles tendon mechanics, including a finite element (FE) model estimating local displacements in the Achilles tendon. However, before implementing this in AT research, further testing and validation is necessary. Therefore, to make a start for future improvements, this study aims to build a foundational FE model of the Achilles tendon, verify it with in vivo local displacement data and assess the sensitivity to subtendon twist.**

3D ultrasound and X-rays of the ankle provided the geometry and the moment arm of the Achilles tendon, respectively. By minimizing the error between the tendon's elongation during contraction and the FE model prediction, the material properties were optimized. Local displacements in the sagittal and coronal plane were computed using estimated forces from in vivo studies. Simulated subtendon twists (11°, 37°, 65°) examined the effect of the amount of twist on the displacement.

Comparing the FE estimated local displacements to in vivo data indicated that additional substructure details are needed to accurately calculate the displacement behavior. Modifying fiber twist angles altered the uniformity of the displacements in the FE model. Therefore, further development of the FE model of the Achilles tendon is recommended before incorporating it into an Achilles tendon mechanics study.

I. Introduction

Tendinopathy in the Achilles tendon, the strongest tendon in the human body, is a common injury in both active and inactive people. In 2011 in the Netherlands about 2.35 per 1000 of the adult patients that were registered by the general practitioner had mid-portion Achilles tendinopathy (AT) [1], [2]. People with tendinopathy have pain in their tendon during tendon-loading activities [3]. In the Achilles tendon, this pain can be located either within the mid-portion region of the tendon, situated 2-7 cm proximal to the calcaneal insertion, or within the initial 2 cm proximal to the insertion, corresponding to the insertion region of the Achilles tendon, or in both regions. In addition to experiencing pain during loading on the Achilles tendon, patients also endure pain during local palpation, accompanied by local swelling [4].

The cause of the injury is not yet clear and for some people current treatments are not successful. About 23 % - 37 % of the patients with AT has some persistent symptoms, which can take up to at least 10 years [5], [4]. Abnormal strain distribution within the Achilles tendon is proposed to contribute to the onset and persistence of AT symptoms [6], [7], [8]. Additionally, there is a suggestion that the amount of twist of the Achilles tendon subtendons (Figure 1) is associated with the distribution of strain in the tendon [9], [10]. However, whether these hypotheses hold true and how it affects the symptoms of the injury remains uncertain.

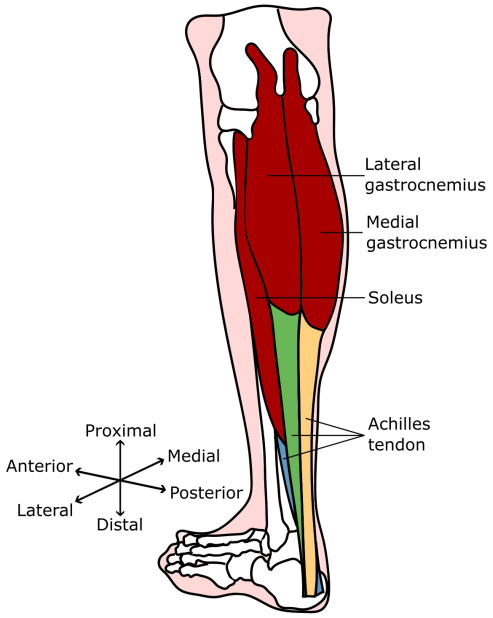

Fig. 1: Visualization of the left lower leg. The Achilles tendon is illustrated, consisting of three subtendons (blue, green and yellow), each originating from one of the triceps surae muscles (red). Towards the calcaneal insertion, the subtendons intertwine, exhibiting a twist. This amount of twist is suggested to influence the strain distribution in the tendon.

To be able to link the displacement behavior of the Achilles tendon of an individual to the development of AT, the influence of different daily-life movements on the tendon has to be examined. Pizzolato et al. (2020) described an integrated framework to study the mechanics of the Achilles tendon of an individual during movement tasks [11]. This framework consists of a neuromusculoskeletal (NMS)

model based on body kinematics and muscle activation of an individual collected during gait analysis with a motion capture system, force plates and surface electromyography sensors. With the NMS model, the force that the triceps surae muscle applied on the Achilles tendon could be estimated. This force could subsequently be applied on a finite element (FE) model of the Achilles tendon, constructed from 3D ultrasound scans captured at rest and during isometric contraction. With this model, local displacements in the tendon could be calculated [12], [11]. To be able to live estimate the displacement distribution in the tendon, a surrogate model giving comparable results as the FE model was created via machine learning approaches [11]. This framework designed by Pizzolato et al. (2020) was only tested with one subject, without validation of the results. Therefore, before such a pipeline can be implemented in research to the development and course of AT, the different parts of the framework have to be further tested and validated.

To be able to choose a surrogate method for the FE model to calculate the local displacement in the tendon, first, a reliable personalized FE model should be built. Therefore, the goal of this research is to construct an FE model of the Achilles tendon, verify it with in vivo local displacement data and evaluate the sensitivity to subtendon twist. This entails building an FE model (Figure 2), using the procedure as described by Pizzolato et al. (2020) as baseline. Subsequently, the model's local displacement calculations were compared to Achilles tendon in vivo data, to test the accuracy of the FE model on this aspect. Additionally, the model's sensitivity to subtendon twist was assessed by applying different fiber angles. Given the reported differences in local displacement behavior between individuals, an additional sensitivity analysis was conducted to evaluate the effect of different material properties on the model's displacement behavior. This analysis aimed to determine whether variations in material properties contributed to discrepancies between in vivo data and FE estimated behavior. By establishing and evaluating this foundational model, the objective is to pave the way for future improvements in the pipeline for studying Achilles tendon mechanics.

II. Method

To create an FE model of the Achilles tendon, the geometry and the moment arm of the tendon of an individual were determined (Figure 2). The extraction of these components was tested with one healthy individual (female, age: 23, mass: 57 kg, height: 164 cm).

A. Geometry of the Achilles Tendon

3D ultrasound, magnetic resonance imaging (MRI) and computerized tomography (CT) are three methods that are suitable to determine the geometry of a tendon. However, the use of CT is less favorable due to its ionizing radiation [13]. Research has shown that 3D ultrasound is a good alternate method for MRI in determining the morphology of the lower limb muscles in vivo [13], [14], [15]. Given its cost-effectiveness and greater accessibility, ultrasound was utilized in this study to determine tendon geometry [14]. 3D ultrasound combines conventional 2D ultrasound imaging with a motion analysis system to create a 3D reconstruction of soft tissue, like tendons, in vivo [16]. The position of the ultrasound probe is recorded by the motion capture system, which makes it possible to merge the different sweeps that are made with the probe after they are transformed to a global coordinate system to reconstruct a 3D volume of the area of interest [17].

During the scan, the subject laid prone on the treatment table, with both feet hanging over the table, the knee joints fully extended and the hip joint in a neutral position. With a

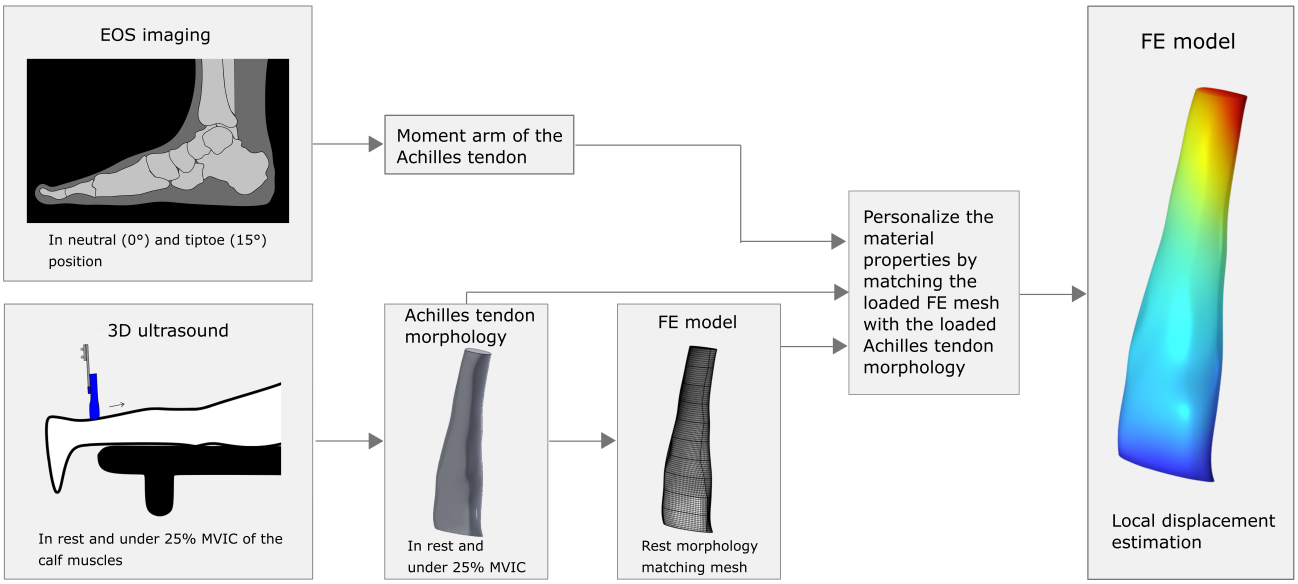

Fig. 2: The pipeline for the development of a finite element (FE) model of the Achilles tendon, based on the framework as described by Pizzolato et al. (2020) [11]. (MVIC = maximum isometric voluntary contraction)

construction, consisting of fixation bands and a dynamometer (MicroFET 2 Hoggan, Hoggan Scientific, USA), the foot that was scanned, was placed and fixated in a light dorsiflexed position, to fully stretch the Achilles tendon (Figure 3). The Achilles tendon was scanned with the ultrasound probe moving in strokes from the insertion point on the calcaneus to the most proximal part of the tendon where the gastrocnemius muscle starts. 3D ultrasound scans can only be captured when the subject remains in a stationary position [11]. Therefore, the ultrasound images were obtained in rest and under isometric contraction of the calf muscles. During the isometric contraction, images were captured when the subject estimated exerting approximately 25% of its maximum voluntary isometric contraction (MVIC). In total the ultrasound images were acquired under two conditions: in rest and under 25% MVIC of the calf muscles. Both conditions were performed twice.

The ultrasound was created combining the Terason Ultrasound System (Terason uSmart 3200T, Teratech, USA) in the default settings to scan an ankle combined with a 10 MHz linear-array transducer (Probe 16L5, Teratech, USA) and a motion capture system (Optotrak Certus; Northern Digital, Waterloo, ON, Canada). A cluster marker was attached to the ultrasound probe as shown in Figure 3 to locate its position and orientation. A Matlab script (Matlab, MathWorks, Natick, MA, USA) was subsequently used to construct an ultrasound voxel array with the data, following the steps described by Weide et al. (2017) [18].

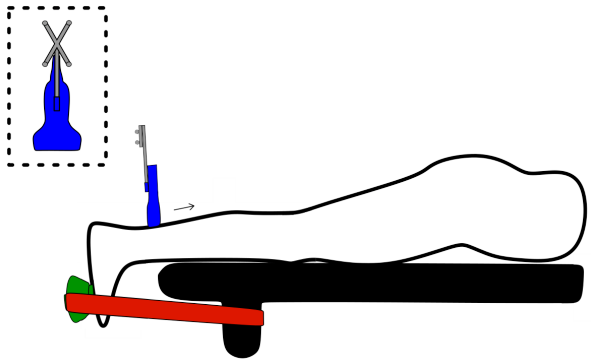

Fig. 3: The set-up during the 3D ultrasound scanning. The subject laid prone on the treatment table (black), with both feet hanging over the table. The knees were fully extended and the hip joint was in a neutral position. The foot that was scanned was placed in a slight dorsiflexion position of the ankle with fixation bands (red). The applied force during the isometric contraction was measured with a dynamometer (green) placed under the heads of the metatarsal bones of the foot. To locate the ultrasound probe (blue), a cluster marker (grey) with four markers was attached to the probe.

With help of the 3D Slicer (Slicer 5.2.2, www.slicer.org, [19]), the geometry of the Achilles tendon was extracted from the ultrasound voxel array [20], [21]. Starting in the most distal slide in the sagittal plane where the Achilles tendon first became visible and ending in furthest slide where the soleus muscle initially appeared, the Achilles tendon was delineated in eleven slides. These slides were evenly distributed along the length and the tendon was selected using the 'Segmentation Editor' tool. The segmentation was subsequently exported as an STL-file and opened in Solidworks (Solidworks 2022, SolidWorks Corporation, USA). Here, the slices were connected by filling the space between them using the 'Loft' tool, creating a reconstruction of the geometry of the tendon.

B. Moment Arm of the Achilles Tendon

To calculate the force in the Achilles tendon during the isometric contraction of the calf muscles, the center of rotation (COR) of the ankle and the moment arm of the Achilles tendon of the subject had to be determined. The EOS system (EOS imaging, France) was used to do this. The EOS system produces X-ray images with a reduced radiation dose, whereby both the anteroposterior and lateral images can be created at the same time with the subject standing in an upright position [22]. Advantages of this technique, compared to MRI, include better accessibility and the capability to capture the ankle in a weight-bearing (standing) position. To measure the Achilles tendon moment arm, the weight-bearing ankle was captured in two positions: a neutral (0°) and a tiptoe (∼15°) position. The tiptoe position induced ankle plantarflexion and dorsiflexion of the metatarsophalangeal joints.

During the scan, the participant stood on the one leg undergoing scanning, with its hands on the support rod. To capture the full foot, the subject was positioned on a plate of about two centimeter thick. The EOS lasers, showing the parts to be scanned, were located just below the standing foot and halfway on the tibia. When the subject was asked to move toward the tiptoe position, the note was given that this movement had to be made as much to the front as possible, to prevent eversion and inversion of the ankle. Whether this movement was performed correctly, was checked with the frontal scan of the ankle. To make sure that the angle that the foot makes with the ground was about 15°, a soft pillow with this angle was placed under the foot, see Figure 4.

The settings of the EOS were set on the lowest possible radiation dose. For both the frontal and sagittal plane this was a dose of 78.88 mGy·cm^2.

The moment arm of the Achilles tendon was subsequently calculated with Reuleaux'geometric method [23]. In this method, the tibia is assumed to be fixed and the talus is the rotating segment. In the scan of the neutral position, two anatomical points (A and B) on the talus were chosen (Figure 5a). To make the direction of the line between these two points more clear, a line of ten centimeter (line AB), parallel to this line was drawn. This was done by creating a construction line of ten centimeter perpendicular to the line through the two anatomical points and proximal to the talus and drawing the direction line AB perpendicular to this construction line, see Figure 5a. The same two anatomical points were identified in the scan with the ankle in plantarflexion position and the same construction was made. This created direction line A_pB_p of ten centimeter, parallel to the line through the two anatomical points on the talus, see Figure 5b.

Fig. 4: The set-up of the EOS scans. The subject was positioned on a 2-cm-tick plate, standing only on the leg undergoing scanning. The tiptoe position was achieved with the assistance of a soft pillow, creating an angle of 15° with the ground.

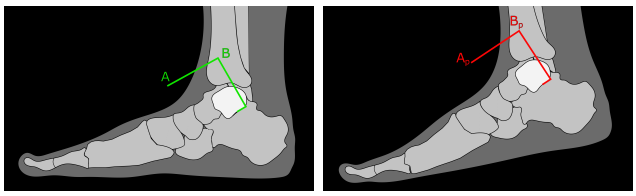

(a) Visualization of the EOS scan of the ankle in neutral position.

(b) Visualization of the EOS scan of the ankle in plantarflexion position.

Fig. 5: Reuleaux'geometric method to determine the center of rotation of the ankle. In the EOS scans of the ankle in neutral and plantarflexion positions, two landmarks on the body of the talus (white) posterior to the lateral process of the talus are selected and the direction of the line between these landmarks is visualized by drawing respectively lines AB and A_pB_p with a length of ten centimeter parallel to this line.

This line construction was subsequently copied to the image of the ankle in neutral position. The COR of the ankle was then defined as the intersection point of line A_pA and B_pB. The moment arm of the Achilles tendon is defined as the perpendicular distance from the line of force of the Achilles tendon to the COR. The line of force of the Achilles tendon was determined by drawing the midline of the Achilles tendon from the insertion point at the calcaneus to a point six centimeter more proximal in the scan of the neutral position of the ankle, see Figure 6.

C. Finite Element Analysis

The local displacements in the tendon were estimated with an FE model. To achieve this, the geometry and the material properties of the tendon were needed. Initially, a mesh, matched with the 3D reconstructed Achilles tendon in rest, was created with COMSOL Multiphysics (COMSOL Multiphysics v. 6.0, COMSOL AB, Stockholm, Sweden). The tendon was modeled as an incompressible, transversely isotropic material [11], [12], [24].

The ground substance hereby was described with a Neo-Hookean model (W_1) and the behavior of the fibers in

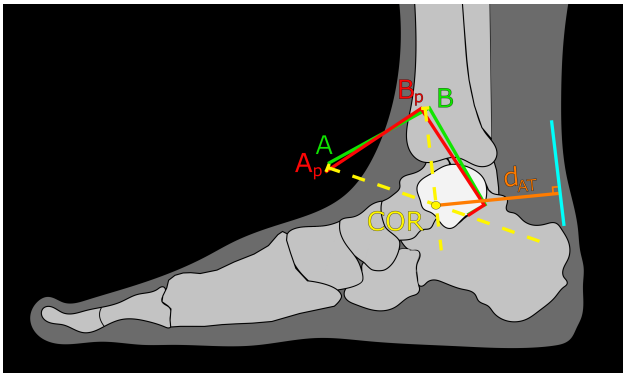

Fig. 6: Visualization of constructions AB (green) and A_pB_p (red), indicating the direction of the body of the talus (white) in, respectively, a neutral and a plantarflexion position of the ankle, both displayed in the scan of the ankle in the neutral position. The center of rotation (COR) is the intersection point of lines A_pA and B_pB (yellow). The line of force was constructed as the midline of the Achilles tendon from the insertion point to a point 6 cm more proximal (blue). The moment arm of the Achilles tendon (d_{AT}) is the perpendicular distance from the line of force to the COR (orange).

the tendon was represented by the Holzapfel-Gasser-Ogden model (W_2). The strain energy functions for W_1 and W_2 are defined by Equation 1 and Equation 2, respectively. The combination of these functions resulted in a total strain energy (W), as outlined in Equation 3 [12], [25], [26].

$$W_1 = \frac{C_1(I_1 - 3)}{2} + \frac{C_2(I_2 - 3)}{2} \tag{1}$$

$$W_2 = 0, I_a < 1 \tag{2a}$$

$$W_2 = \frac{k_1}{2 \cdot k_2}(e^Q - 1), I_a \geq 1$$

$$Q = k_2 \cdot (k_3(I_1 - 3) + (1 - 3 \cdot k_3)(I_a - 1))^2 \tag{2b}$$

$$W = W_1 + W_2 \tag{3}$$

In these expressions, I_1 and I_2 represent the first and second invariants of the right Cauchy stretch tensor, while I_a denotes the squared value of the isochoric elastic stretch in the fiber direction. The coefficient C_1 describes the second Lamé parameter and was estimated based on measurements on cadaver tendons: C_1 = 61.098 N/mm^2 [27], [28]. To create the Neo-Hookean model, coefficient C_2 was set equal to 0 [26], [27]. The parameters k_1 and k_2 represent the fiber stiffness and a dimensionless parameter, respectively [29]. These values were also established based on cadaver experiments, with k_1 set to 327.345 MPa and k_2 to 0.01 [27], [28]. The fiber dispersion is described by k_3. Assuming that all the fibers are oriented in the same direction, k_3 was equalized to 0 [26]. The direction of the fibers was set to create a torsion of 37° in the tendon, as observed in cadavers by Van Gils et al. (1996) [30].

The most distal nodes of the FE model were fixed to remain stationary, while the force generated by the soleus, gastrocnemius medialis, and gastrocnemius lateralis muscles was applied to the most proximal surface, see Figure 7 [11].

The applied force on the tendon was determined with Equation 4. Herein represents $F_{applied}$ the measured force of 25% MVIC during the isometric contraction, $d_{applied}$ the distance between this measured force and the center of rotation as determined with the X-ray and d_{AT} the moment arm of the Achilles tendon. It was assumed that 83% of the total applied force originated from the soleus and gastrocnemius muscles, thereby effecting the Achilles tendon [27], [31].

Fig. 7: On the most proximal face of the Achilles tendon FE model, the estimation of the force produced by the triceps surae muscle was applied, evenly distributed over the surface. The most distal face of the model (blue) was fixed on its place.

$$F_{AT} = 0.83 \cdot F_{applied} \cdot \frac{d_{applied}}{d_{AT}} \tag{4}$$

To find the optimum mesh element size, the number of mesh elements whereby displacement and Von Mises stress differences between two consecutive analysis were less than 5% on all those nodes from the model with a smaller element size was assumed to be acceptable.

The parameters C_1, k_1 and k_2 were optimized by using an iterative approach to personalize the material properties. Hereby the values that would provide the best match between the loaded FE mesh of the Achilles tendon and the geometry of the equally loaded Achilles tendon measured with 3D ultrasound were searched [11]. For this, the $fmincon$ function in Matlab (Matlab Version R2020b, The MathWorks, Natick, MA, USA) was used to optimize C_1, k_1 and k_2 parameters by minimizing the root-mean square error (RMSE) between the measured tendon displacement and the FE estimated one.

Additionally, the model's behavior with these material properties was examined by analyzing whether the stress-strain curve of a cylinder with the same model and parameters showed a linear or nonlinear trajectory up to the stress induced by the applied force.

D. Model Verification

Stenroth et al. (2019) conducted in vivo measurements of local displacements in Achilles tendons in both the sagittal and the coronal plane. Fourteen healthy adults (5 female and 9 male, age: 26±3 years, mass: 75.3±10.2 kg, height: 180±8 cm) participated, performing maximal voluntary isometric ankle plantarflexion contractions in two conditions: with the knee extended and with the knee in a 110° flexion position. Ultrasound scans in both planes were taken, and the displacement was measured at 16 uniformly spaced nodes distributed over 15 mm in the longitudinal direction of the tendon in each of six regions of the tissue. These six regions were evenly distributed over the depth in the sagittal plane and the width in the coronal plane of the Achilles tendon. Measurements were taken between the tendon at rest and under isometric contraction. The peak displacements were averaged for each region and normalized by dividing the mean displacement in the specific region by the mean displacement across all regions [32].

To test whether the FE model accurately represents the local displacement behavior observed in in vivo tendons, the Achilles tendon FE model was compared with data reported by Stenroth et al. (2019). To evaluate this, the mean force applied by the subjects of Stenroth et al. (2019) was recalculated with the measured moment arm and applied on the FE model. The sagittal and coronal planes were reconstructed in the FE model based on a figure shown in the Supplementary file of Stenroth et al. (2019). The cross-sections of these planes in the FE model were segmented into six regions, and across a 15 mm section in the longitudinal direction of the tendon, 16 uniformly spaced nodes were positioned in each region, following Stenroth's methodology [32]. Hereby the most proximal nodes were placed at a distance 10% of the total tendon length from the proximal surface of the tendon model. A visualization of the placement of the nodes in the model in the sagittal plane is given in Figure 8. The normalized data from Stenroth et al. (2019) that was measured in the position with the knee extended, from now on also referred to as 'in vivo data', was compared to the, in the same way averaged and normalized, displacement measured in the FE model [32]. Given that individual subjects in Stenroth et al.'s study showed varying displacement behavior in their Achilles tendons, it was tested whether the FE model estimated behavior of the displacement in the Achilles tendon inside one standard deviation of the mean measured in vivo [32].

E. Model Sensitivity

To further evaluate the FE model, two sensitivity analyses were conducted. First, a sensitivity analysis was carried out to determine the influence of the amount of twist of the subtendons on the FE model. The twist of the fibers in the FE model, initially optimized at 37°, was modified to 11° and 65°, representing the reported range of mean twist in tendons observed by Van Gils et al. (1996) [30]. Whether the normalized nodal displacements in the FE models with different twists gave similar results in comparison to in

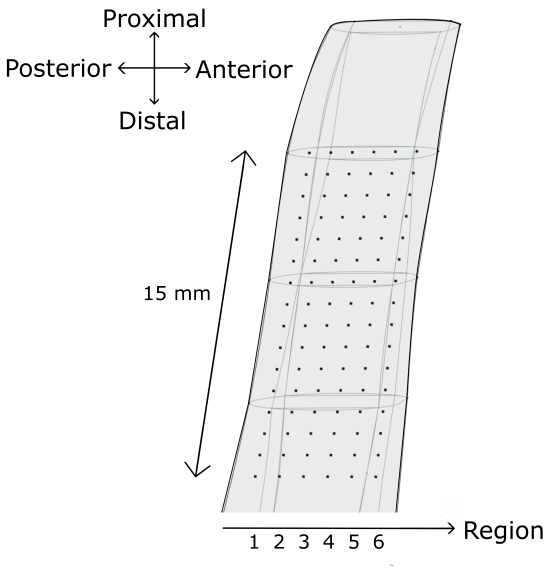

Fig. 8: Visualization of the placement of the nodes in the sagittal plane of the tendon model for the verification. In the posterior/anterior direction, the tendon was divided in six regions. In each of these six regions, 16 nodes were uniformly distributed over 15 mm in the longitudinal direction of the Achilles tendon.

vivo tendons as reported by Stenroth et al. (2019) was analyzed by performing an intuitive trend analysis. This involved comparing the trajectory of the graphs representing the behavior of the FE models with those of the in vivo data from the individual subjects by plotting them side by side [32]. Next to this, to compare the effect on the local displacement behavior of the models with different twist angles, the average deviation from the course of the graph of the model with a twist angle of 37° was examined by calculating the root-mean square deviation (RMSD) of the FE estimated values with twists angles of 11° and 65° from the FE model with a twist angle of 37°.

Secondly, because the local displacement behavior in the tendon varies per individual, the sensitivity of the model to the personalized material parameters C_1, k_1 and k_2 was also studied to determine whether variations in material properties contributed to discrepancies between in vivo data and FE estimated behavior [32]. To analyze the effect of these parameters, models were created with one of these parameters adjusted to 33.3%, 75%, 125% and 300% the personalized value while keeping the other parameters constant. The estimated local displacement behavior of these models was subsequently analyzed by plotting the values next to the data from the individual subjects of Stenroth et al. (2019) and calculating the RMSD of the model from the FE model with the personalized material properties [32].

III. Results

To receive a good mesh quality, the mesh of the Achilles tendon FE model consisted of both hexahedral elements and triangular prisms, see Figure 9. As the result of the convergence analysis, the mesh consisted of 62 640 elements.

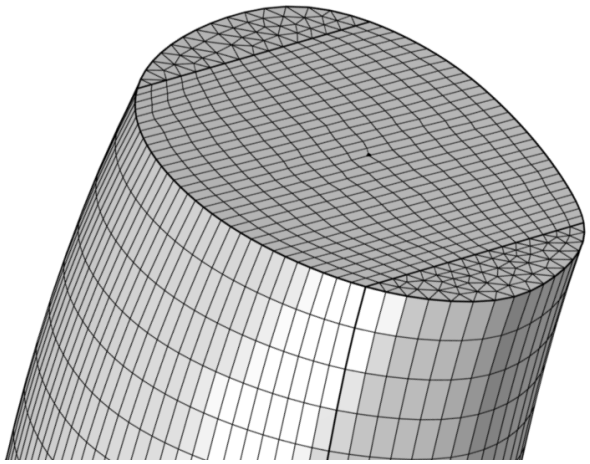

Fig. 9: The mesh consisted of triangular prism elements at the lateral and medial sides of the tendon geometry with in between hexahedral elements.

After optimizing the material properties C_1, k_1 and k_2, the minimal RMSE between the predicted displacement in the tendon and the actual displacement under 25% MVIC was found at the material properties $C_1 = 96.6048$ MPa, $k_1 = 320.7504$ MPa and $k_2 = 0.0265$. At this optimum, the total elongation of the FE model differed by 8.9% from the measured elongation of the tendon.

With the cylinder geometry, the model showed an approximately linear stress-strain curve up until the load as applied on the Achilles tendon model (Appendix A).

A. Model Verification

In both the sagittal and coronal planes, the local displacement showed a non-uniform behavior. In the sagittal plane, the displacement increased from the most posterior to the anterior region, while in the coronal plane it increased from the most lateral to the medial regions from the tendon (Figure 10A, Figure 11A). In the sagittal plane, the normalized displacements in the regions fell within one standard deviation of the mean normalized displacement as reported by Stenroth et al. (2019). However, in the coronal plane, the displacement behavior deviated by more than one standard deviation from the reported mean in vivo. See Figure 10A and Figure 11A for these comparisons of the normalized displacement data of the FE model with the in vivo data.

B. Model Sensitivity

The displacement behavior with twist angles of 11° and 65° deviated, on average, by 0.034 and 0.035, respectively, from the model with a twist angle of 37° in the regions in the sagittal plane, as detailed in Table I. The FE model with a twist angle of 11° hereby showed a flatter trajectory, whereas the FE model with a twist angle of 65° displayed a steeper trajectory compared to the trajectory of the FE model with

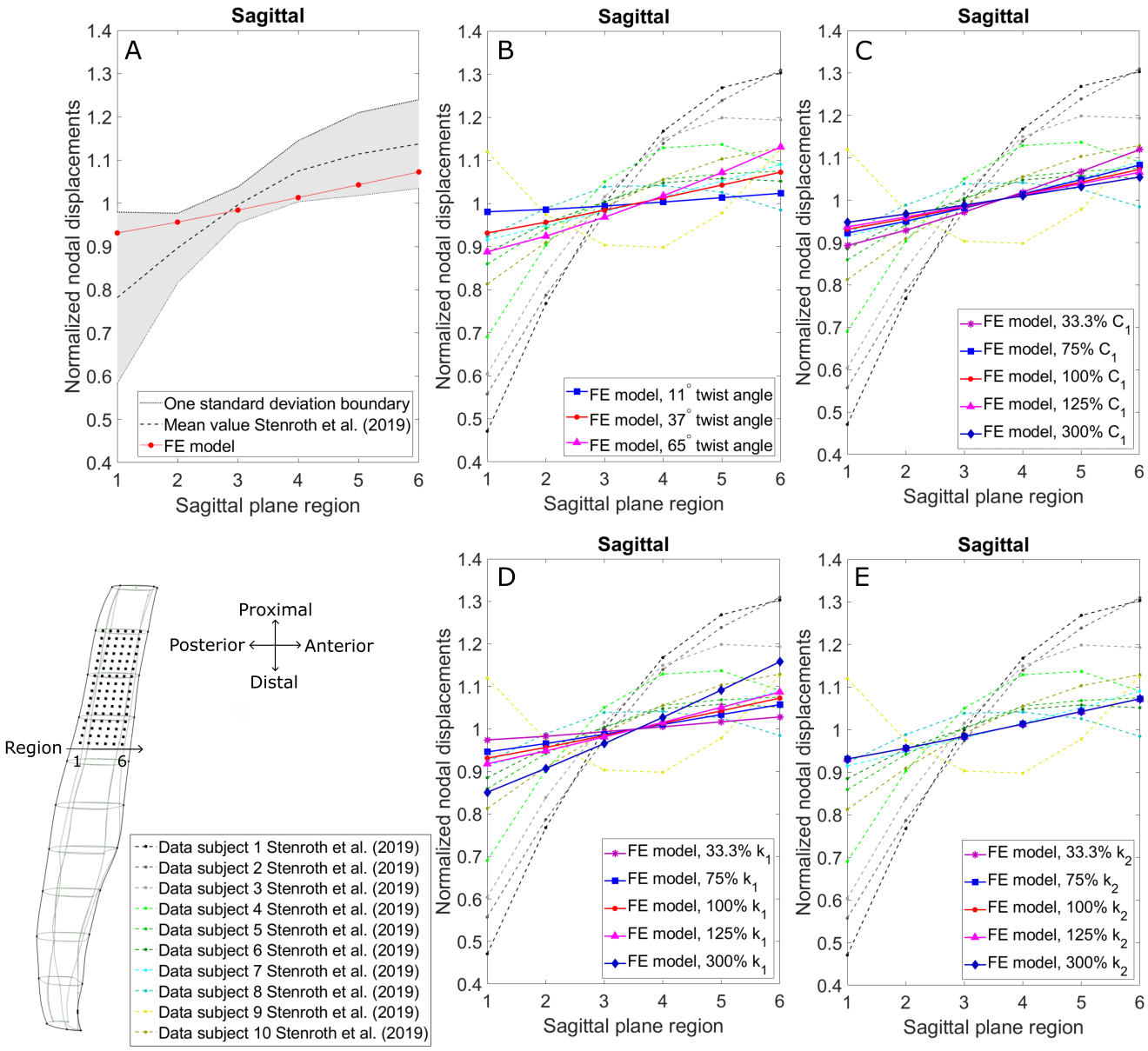

Fig. 10: Mean displacement of the nodes in six regions in the sagittal plane, normalized by the average displacement of all regions and compared to reported in vivo data [32]. A: Finite element (FE) model compared to mean and standard deviation in vivo data. B-E: The sensitivity of the FE model to the twist angle, parameters C_1, k_1 and k_2, respectively, compared to in vivo data from individual subjects. In the left lower corner a visualization of the placements of the nodes of each region in the sagittal plane of the FE model is given. Region 1 is hereby the most posterior region in the plane of the tendon.

a twist angle of 37° (Figure 10B). While the trajectory of the model with a twist angle of 37° approximately followed the trajectory of subject 7 from Stenroth et al. (2019), the FE models with adjusted twist angles do not seem to display behavior similar to one of the subjects from Stenroth et al. (2019), as seen in Figure 10B.

In the coronal plane, the RMSDs of the FE models with 11° and 65° twist angles in comparison to the model with a twist angle of 37° were 0.003 and 0.005, respectively (Table I). Similar to the sagittal plane, the model with a twist angle of 11° estimated a flatter trajectory of the displacements across the regions and the model with a twist angle of 65° showed a steeper trajectory across the regions compared to the behavior of the model with a twist angle of 37° in the coronal plane (Figure 11B). Comparing the behavior of the FE models with different twists to the data of the individual subjects from Stenroth et al. (2019) showed that none of the models showed a trajectory similar to any of the subjects, as seen in Figure 11B.

Regarding the personalized material properties, the displacement behavior of the FE model was most sensitive to adjustments in the k_1 parameter, followed by parameter C_1. The model was the least sensitive for changes in the k_2 parameter, as inferred from the RMSDs in Table I. The FE models with values of 125% of the optimized k_1 and 75% of the optimized C_1 closely followed the trajectory of subject 7

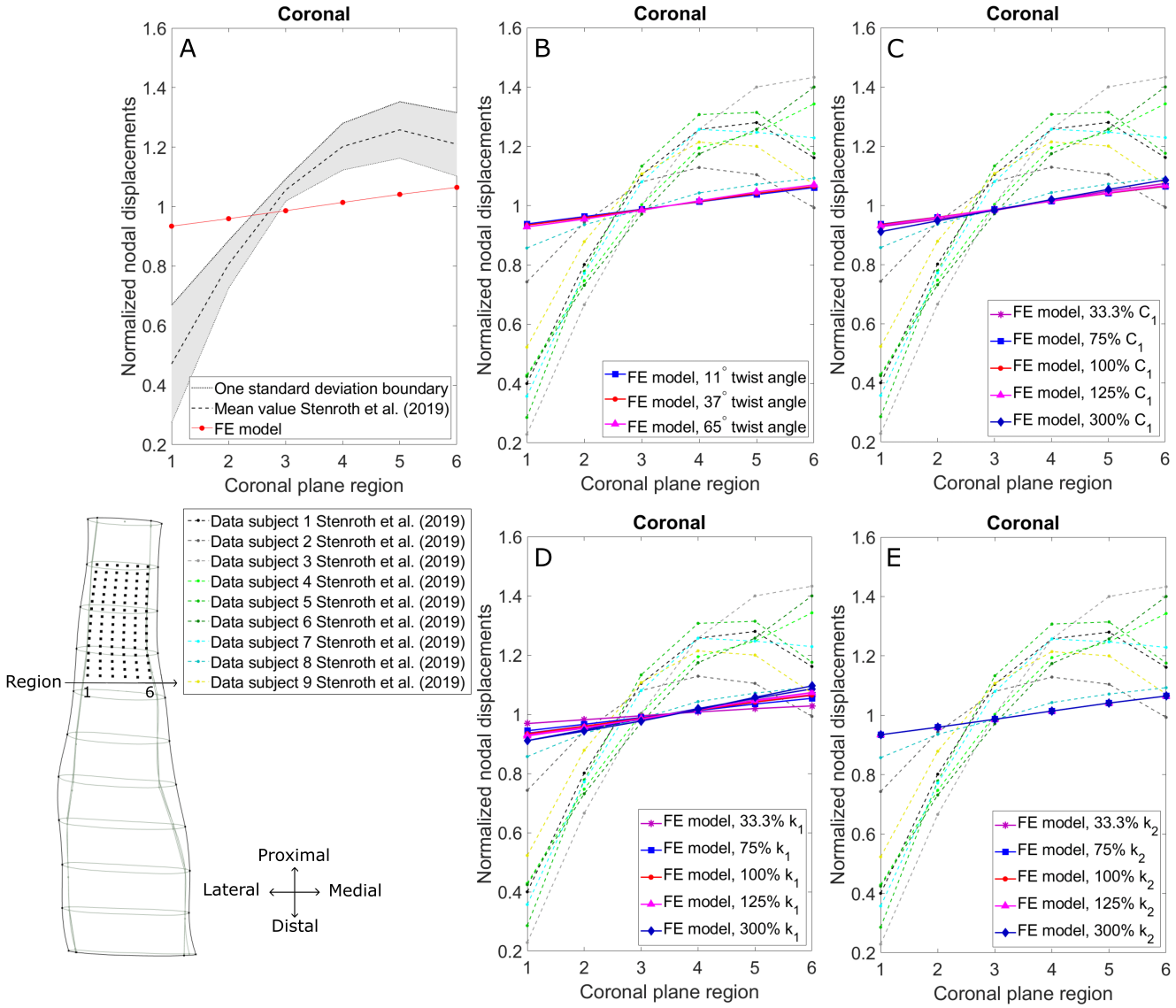

Fig. 11: Mean displacement of the nodes in six regions in the coronal plane, normalized by the average displacement of all regions and compared to reported in vivo data [32]. A: Finite element (FE) model compared to mean and standard deviation in vivo data. B-E: The sensitivity of the FE model to the twist angle, parameters C_1, k_1 and k_2, respectively, compared to in vivo data from individual subjects. In the left lower corner a visualization of the placements of the nodes of each region in the coronal plane of the FE model is given. Region 1 is hereby the most lateral region in the plane of the tendon.

in the sagittal plane (Figure 10). In the coronal plane, none of the conditions showed displacement behavior similar to one of the in vivo subjects (Figure 11). Despite adjustments in parameter values, the model maintained an approximately linear trajectory in the normalized displacement between regions in both the sagittal and coronal planes (Figure 10, Figure 11).

IV. Discussion

The aim of this research was to build a foundational FE model of the Achilles tendon, verify it with in vivo local displacement data and evaluate the sensitivity to subtendon twist. The created model estimated normalized local displacements of the nodes in the sagittal plane that fell within one standard deviation from the mean as reported in in vivo tendons. However, the calculated normalized local displacement of the nodes in the coronal plane showed displacement behavior that fell outside one standard deviation from the measured mean in vivo in all regions. Decreasing the amount of twist of the fibers in the tendon model led to a flatter trajectory of the displacement behavior across the regions, whereas an increased amount of fiber twist showed a steeper trajectory. This difference was particularly prominent in the sagittal plane, with minimal variation observed in the coronal plane.

Despite falling inside one standard deviation of the reported in vivo mean, the trajectory of the displacement behavior in the sagittal plane does not approximate the mean behavior as reported in vivo (Figure 10A). However, when the local displacement estimations of the FE model are

FE model	Sagittal plane	Coronal plane
11° twist angle	0.034	0.003
65° twist angle	0.035	0.005
33.3% C_1	0.0294	0.0062
75% C_1	0.0066	0.00076
125% C_1	0.0043	0.0015
300% C_1	0.0119	0.0149
33.3% k_1	0.0298	0.0245
75% k_1	0.0103	0.0072
125% k_1	0.0094	0.0055
300% k_1	0.0564	0.0189
33.3% k_2	$1.32{\cdot}10^{-6}$	$8.65{\cdot}10^{-7}$
75% k_2	$4.96{\cdot}10^{-7}$	$3.24{\cdot}10^{-7}$
125% k_2	$4.96{\cdot}10^{-7}$	$3.24{\cdot}10^{-7}$
300% k_2	$3.97{\cdot}10^{-6}$	$2.59{\cdot}10^{-6}$

TABLE I: Root-mean square deviation (RMSD) of the displacement in the regions normalized by the average displacement of all regions, of the models with an adjusted twist angle or adjusted parameter C_1, k_1 or k_2 from the model with a twist angle of 37° and parameters optimized to match the elongation of the tendon as measured with 3D ultrasound.

compared to the data from individual subjects, it roughly follows the trajectory of subject 7 in the sagittal plane (Figure 10B). This observation emphasizes the variations in displacement behavior in the Achilles tendon among individuals as reported by Stenroth et al. (2019) [32]. Given that the FE model is based on data from one single subject, the estimated values from the model were therefore not expected to follow the in vivo mean displacement behavior. Adjusting the parameters C_1 or k_1 to 75% C_1 or 125% k_1, respectively, made the behavior of the FE model in the sagittal plane follow the trajectory of subject 7 more closely (Figure 10C and Figure 10D). However, despite the fact that adjusting the material properties led to a modification in the local displacement trajectory, the different conditions did not lead to an approximation of a trajectory of one of the other subjects in the sagittal plane. In the coronal plane, no condition of the material properties significantly changed the trajectory of the displacement behavior to align with one of the curves reported by the individual subjects in vivo (Figure 11). A reason for this was that, despite the fact that the models with a twist angle of 65° and 300% k_1 showed a slightly more nonlinear trajectory over the regions in the sagittal plane, the estimated local displacement behavior of the FE model remained approximately linear in every condition over the regions in both the sagittal and coronal plane. In contrast, a nonlinear curve of displacement behavior was reported in vivo by some of the individual subjects in the sagittal plane and all subjects in the coronal plane. Next to this, the slightly nonlinear behavior in the sagittal plane of the FE models with a 65° twist angle and 300% k_1, does not seem to approximate the behavior as reported in the individual subjects that showed nonlinear displacement behavior over the regions.

A possible explanation for these differences in behavior between the FE model and the in vivo data could be attributed to the geometry of the tendon. Hansen et al. (2017) drew the conclusion that tendon geometry significantly influences stress distribution in an Achilles tendon model, suggesting that the specific geometry of the Achilles tendon in the subject being studied may play a role in the displacement behavior and therefore may contribute to variations in outcome between the FE model and in vivo data [12]. That the model with a cylinder geometry exhibited an approximately linear stress-strain curve up until the load as applied on the Achilles tendon FE model, indicates that the model behaves approximately linear with its initial parameters. Therefore, the outer shape appears to have minimal influence on the linearity of the displacement behavior in this case.

Another reason for the model's deviation in local displacement behavior from the in vivo data could be that the subtendons of the tendon are not individually modeled in current FE model, thereby preventing sliding between these components. The Achilles tendon consists of three subtendons: one of each triceps surae muscle (Figure 1). Both the reported difference in displacement between the aponeuroses of the soleus and medial gastrocnemius muscle proximal to the Achilles tendon junction and the observation of sliding between subtendons in the Achilles tendon of rabbits, suggest sliding of the subtendons in the human Achilles tendon [33], [10]. Both Handsfield et al. (2020) and Diniz et al. (2023) reported this sliding to be an important factor in causing the non-uniform displacement behavior in the Achilles tendon [33], [27]. These conclusions find support in the observed differences in elongation of the subtendons of the soleus and the medial and lateral gastrocnemius muscles in vivo [34], [35]. Diniz et al. (2023) investigated this by comparing FE models with and without sliding between the subtendons. Their model without sliding showed an approximately linear trajectory of displacement behavior, while enabling sliding in the model resulted in more nonlinear displacement trajectories in both the sagittal and coronal plane [27]. Due to time constraints, this enhancement has not yet been implemented as an improvement in the current FE model. Nevertheless, considering the inadequate estimations of the local displacements of current FE model and the findings of Handsfield et al. (2020) and Diniz et al. (2023), the incorporation of such modeling will be valuable. Apart from the type of contact (frictionless, anisotropic friction, etc.) between the subtendons, this sliding mechanism in general form can be incorporated by splitting the reconstruction of the Achilles tendon geometry in three subtendons, based on information from cadaver studies [33], [27]. However, implementing personalized, separate subtendons in the FE model will be more complex. For this, the geometries of the subtendons and how they relate to each other should be determined. At present, achieving clear visualization of these forms through ultrasound remains challenging. Szaro et al. (2020) concluded that locating the subtendons with MRI is hard and only the subtendon of the lateral gastrocnemius is commonly found [36]. As an alternative, until a reliable imaging method is identified to distinguish the subtendons, considering incorporating the three calf muscles during the acquisition of the 3D ultrasound scan could be explored. The ratio in cross-sectional area among the muscles could then possibly be utilized to estimate the distribution of the cross-sectional area of the Achilles tendon across its subtendons.

If this method gives realistic results when compared to cadaver data from Achilles tendon subtendons, it is proposed that this will be incorporated in future research on Achilles tendon FE models and that the effect of different types of contact between the subtendons on the validation of local displacement will be studied.

Related to this is another notable simplification in the framework that could justify the observed differences in displacement behavior between the model and in vivo data; the equal distribution of the forces produced by the triceps surae muscle on the proximal face of the tendon. Albracht et al. (2008) reported differences in capabilities of maximal force production among the three muscles [37]. The capacity of maximal force production of a muscle is proportional to the physiological cross-sectional area (PCSA) [37], [38]. Considering the reported significance of applied force in influencing displacement variations, the utilization of forces based on the PCSA of the muscles is likely to impact nodal displacements and would therefore improve the reliability of the FE model of the Achilles tendon [33]. With adding scanning the triceps surae muscle during the acquisition of the 3D ultrasound scan, this aspect could be incorporated in the framework.

Regarding the applied force, also the assumption was made that 83% of the plantarflexion force was produced by the triceps surae muscle and therefore was applied on the Achilles tendon. Using a personal NMS model could help determining the contribution of each of the calf muscles to produce a certain force, like the plantarflexion force, more precise. This would improve the determination of the material properties and enable a more accurate replication of the measured force during movement tasks within the model. The development of an individualized NMS model, as outlined by Pizzolato et al. (2020), is a crucial step within the investigative pipeline aiming to analyze the mechanical properties of the Achilles tendon during movement tasks. Constructing such a model requires detailed information regarding bone and muscle geometries, along with neuromuscular parameters of an individual [11], [39], [40], [41]. While the NMS model, as conceptualized by Pizzolato et al., requires further testing and validation, the creation of an individualized NMS model is a labor-intensive process [11]. Therefore, it is recommended to temporarily defer combining an FE model with an NMS model for further testing and validation of the FE model.

Considering the results in the coronal plane, it should be noted that Stenroth et al. (2019) did not measure their results in this plane exactly perpendicular to the sagittal plane. This, along with the observation reported in the Supplementary file of Stenroth et al. (2019) that the position of the probe does influence the results and the absence of a reported exact angle that the coronal plane made with the sagittal plane in Stenroth's research, might also be a factor contributing to the differences between the FE model and the in vivo data [32]. Next to this, the fact that Stenroth et al. (2019) did not report the exact longitudinal location in the Achilles tendon of their measurements has to be considered while evaluating the results of the model verification. Handsfield et al. (2020) found that the variation between local displacements in the tendon was greater more proximal in the tendon, which implies that the measurement location in the longitudinal direction of the tendon does influence the behavior [33]. Based on the information in the Supplementary file from Stenroth et al. (2019) that the location of the images was close to the muscle-tendon junction, the location of most proximal nodes in the FE model was set about 10% of the total length distal to the most proximal surface of the tendon model [32].

In the sagittal plane, the displacement of the nodes was bigger in the more anterior regions compared to the posterior regions. This is in accordance with data reported in multiple in vivo studies [32], [42], [43]. The nodal displacement in current FE model increased from the lateral regions to the medial regions of the tendon in the coronal plane, which is also a similar behavior of the displacement as reported in vivo [32].

Comparing the FE model with the no-sliding model from Diniz et al. (2023) showed that current model estimates local displacements in the sagittal plane more accurately, falling within one standard deviation of the mean as reported in vivo [27]. A difference between the two models is that Diniz et al. (2023) did not personalize their FE model in terms of material properties. Supported by the results of the sensitivity analysis of material properties C_1, k_1 and k_2, in which particularly modifying parameters k_1 and C_1 resulted in alterations in the displacement behavior, this suggests that personalizing the FE model's material properties significantly improves accuracy.

The sensitivity analysis revealed that a small twist angle resulted in more uniform displacement behavior, highlighting the importance of implementing a subject-specific twist of the subtendons in the model to calculate reliable displacements. However, as mentioned before, the identification of the Achilles tendon subtendons in images is currently unsatisfactory, limiting measuring individual subtendon twists [44]. Therefore, more research to possible methods to capture this twist is needed before it can be implemented in the framework.

Comparing the sensitivity results between the coronal and sagittal planes, it was observed that the effect of an adjusted twist angle was minimal in the coronal plane. Concerning sensitivity to the material properties, similar RMSDs to those observed in the sagittal plane were only found in the coronal plane with the lowest measured ratios between the stiffness of the fibers (k_1) and the shear modulus of the ground substance (C_1). Notably, increasing the shear modulus (300% C_1) resulted in a more nonuniform trajectory of the displacement behavior in the coronal plane, in contrast to the sagittal plane. The differing outcomes of the sensitivity analyses in the sagittal and coronal planes could be attributed to the FE model's shape. However, the precise influence of the geometry, in conjunction with fiber twist and material parameters, of an FE model on displacement behavior differences across the two anatomical planes remains unclear. Therefore, if this discrepancy persists with the incorporation of a more detailed substructure in the FE model and inaccurate results persist

in one of the planes, further investigation is advised.

In addition to the aforementioned factors, there are some other points on which the development of the FE model could be improved. While 3D ultrasound imaging is a reliable method to scan human muscle tissue, the experimental set-up is crucial to reduce the noise in the images. Due to incorrect dimensions of the sensor-holder that secured the movement-tracking sensor to the probe, the sensor could slightly move during the scanning, leading to reduced quality of the 3D ultrasound scans. Moreover, the construction for the measurement of the applied force was not strong enough to handle the MVIC or even 50% of the MVIC. With a more steady construction, more scans could be made under different circumstances. Suggested is to add measurements under 50% and 70% MVIC, because a bigger applied force would lead to larger displacements in the tendon. Due to a constant amount of spacing between two consecutive ultrasound images in the longitudinal direction, a bigger displacement would lead to a more accurate estimation of the strain in the tendon based on the scans. Because the in vivo elongation could be measured more precisely, this would make it possible to estimate the material properties more accurately and therefore would lead to a more reliable model. Measuring the strain of the tendon under multiple forces would also create the opportunity to test the accuracy of the FE model. This can then be achieved by comparing the strain estimates of the optimized model with the measured strain from ultrasound scans conducted under these different forces.

For the estimation of material parameters C_1, k_1 and k_2, a gradient based optimization method was used. It is possible that the found values cause a local minimum of the RMSE. To maximize the probability that during the optimization the desired global minimum of the RMSE was found, the values found in literature were used as initial values [27], [12], [28].

While building the FE model of the Achilles tendon, the assumption of the material parameters of the tendon to be homogenous was made. However, considering reported variations in material properties between ex vivo subtendons, it is plausible that differentiation in local properties could impact local variation in displacement in the human Achilles tendon [45]. This could be studied by using shear wave elastography to measure the shear wave speed in the tendon. The shear wave speed is in transversely isotropic materials such as the Achilles tendon dependent on the shear elastic modulus, which results in more insights in the local material parameters [46], [47], [48]. Shear wave velocity is higher in stiffer tissue and is directly proportional to tissue stiffness [49]. With this information, local variation in material parameters could be added to the model. This could be integrated in the framework by adding extra scans of the Achilles tendon of the foot with an ultrasound system in sonographic mode [50]. However, an important limitation of the use of elastography on the Achilles tendon is that current available systems have a much lower maximum output value than the expected elasticity of healthy tendons [48], [50], [51]. This will lead to underestimated outcome values of the stiffness. At present, the available shear wave elastography technique does not exhibit sufficient reliability with regard to local material properties to contribute significantly to the construction of a reliable FE model of the Achilles tendon. Therefore, further improvement of this technique for this application is recommended and till then its incorporation into the pipeline is not advised. An alternative approach to potentially incorporate local material properties into the FE model globally could involve comparing the strain of the various subtendons in the ultrasound with the strain of the subtendon in the FE model. This would allow for the independent optimization of the material properties of each subtendon, thereby refining the model. To measure the elongation of the subtendons, the most distal parts of the soleus, medial gastrocnemius and lateral gastrocnemius should be identified in the ultrasound. Although this method neglects potential differences in material properties between the Achilles tendon distal and proximal to the junction with the soleus, as well as the variation in twist of the subtendons among individuals, it appears to be a method to roughly incorporate local variations in material properties into the model. Further research is essential to determine the true significance of this addition to the model.

In the human body, the Achilles tendon is surrounded by other parts of the human body, which makes it plausible that the human tendon cannot freely move in every direction. Despite this, the only movement constraint that was set on the FE model was the constraint of the most distal face to remain on its place. Applying the force in the elongation direction of the FE tendon did cause displacements in the same direction, but by constraining the proximal surface to only move in the direction of the applied force, a more realistic environment can possibly be created in the FE model [27]. As described by Diniz et al. (2023) this can be added to an FE model build in Abaqus 6.14 (Dassault Systèmes) [27]. To implement such a constraint in an FE model built in COMSOL, an option would be to incorporate a rigid and fixed box around the tendon with high stiffness. This box has to follow the shape of the tendon model with only leaving space in the elongation direction of the tendon (at the most proximal face of the model) for the model to move. The elongation direction of the tendon can be determined with the 3D ultrasound scans in rest and under contraction. A drawback of this feature will possibly be that it will increase the simulation time of the FE model.

Another limitation of the methodology used to create the FE model is that manually selecting the Achilles tendon from the 3D ultrasound scans to create a segmentation of the geometry is time extensive work and decreases the repeatability of the study. Hansen et al. (2017) concluded in their FE analysis that the geometry of the Achilles tendon model influences the stress distribution in the tendon [12]. This indicates that the geometry also affects the displacement behavior. Therefore, to accurately compare and study the displacement behavior in tendons of different individuals, using a method with which the segmentation from the ultrasound would be automated would be useful. Cunningham et al. (2016) described an auto-segmentation method for five bilateral cervical muscles [52]. Making this method

suitable for the segmentation of the Achilles tendon would be valuable.

Next to this, the strain energy density function of the fibers in the FE model was represented by the Holzapfel-Gasser-Ogden model. This model is originally designed to model the anisotropic mechanical behavior in arteries, but is often used to describe soft tissues in the human body like the Achilles tendon [27], [26], [53]. However, many other studies used a model designed for ligaments as described by Weiss et al. (1996) to compute the strain energy of the collagen fibers of the Achilles tendon [11], [12], [28], [25]. It is unclear whether one of these models is a better fit for modeling the Achilles tendon. As neither of them is explicitly designed for tendon modeling, it is conceivable that both may fall short in capturing the precise behavior of the Achilles tendon. Additionally, even though the elastic behavior in the Achilles tendon is more prominent compared to the viscous behavior, the use of a hyperelastic model for the Achilles tendon neglects the viscoelastic behavior of the Achilles tendon [54], [55], [56]. This aspect will be important for the model when the FE model will be implemented in a pipeline to study the behavior of the Achilles tendon during dynamic movements, as proposed by Pizzolato et al. (2020) [11]. A better fitting model could give better insight in the local deformations in the tendon.

With k_3=0, assumed is that all the fibers are oriented in the same direction. Currently, there is no data about the fiber dispersion in the Achilles tendon, but Kadlowec et al. (2009) described a way to determine the fiber orientation with polarized images in cadavers [27], [57], [58]. The finding that the displacement behavior of the FE model is sensitive to changes in the amount of twist, and therefore the fiber angle in the tendon, combined with the reported sensitivity of local displacements in an FE tendon model to this dispersion parameter highlights the potential improvement in the FE model by incorporating data from the Achilles tendon in the model [27]. Examining the fiber dispersion in the Achilles tendon through the analysis of cadaver tendons is therefore valuable.

Considering the results, it is important to address the limited sample size, consisting of only one subject. To be able to investigate whether the pipeline provides an FE model that accurately represents various types of in vivo tendons, a bigger group of subjects is needed. With Edama et al. (2014) categorizing tendons in three different types that describe amounts of twists of the subtendons, and the least common type occurring in 7% of the cases, a minimum sample size of 15 subjects could be justified to increase the likelihood of representing all various types of tendons in the study [59]. Additionally, adding in vivo displacement measurements of the same subjects for comparison with FE model estimations can be valuable due to individual variability in displacement behavior. Conducting those in vivo displacement measurements alongside the development of a personalized FE model for a larger group is time-intensive; however, a compromise could involve validating individual FE models against previously reported in vivo data and additionally measuring in vivo displacements for at least three randomly selected participants to compare against their respective FE model estimations.

V. Conclusion

In this study a foundational FE model of the Achilles tendon was created and evaluated in terms of local displacement estimation. From the findings of this research can be concluded that:

- The FE model of the Achilles tendon that was created did estimate the behavior of the local displacement in the sagittal plane inside one standard deviation from the mean as reported in in vivo Achilles tendons.
- However, to accurately calculate the nonlinear nodal displacement behavior over the regions in both the sagittal and coronal planes as reported in vivo, additional details of the substructure of the Achilles tendon should be incorporated into the FE model.
- The amount of fiber twist in the FE model of the Achilles tendon that was created altered the displacement behavior, with a smaller angle resulting in a flatter trajectory of nodal displacements across the regions within the depth of the FE tendon model.

Therefore, further development of FE models is required to accurately estimate the local displacement in the Achilles tendon before incorporating it into a pipeline for studying individual Achilles tendon mechanics.

Acknowledgements

I want to acknowledge my supervisors, Dr. ir. Eline van der Kruk, Dr. ir. Nazli Tümer and Dr. Robert-Jan de Vos for their guidance throughout this research project. I want to thank Dr. Guido Weide for informing about and making available of the 3D ultrasound and Leslie Bujoczek - van Geest for her efforts which enabled the incorporation of the EOS scans in the research. Lastly, I also want to acknowledge my participant for contributing her time and data to this study.

References

[1] S. K. Williams and M. Brage, "Heel pain—plantar fasciitis and achilles enthesopathy," *Clinics in sports medicine*, vol. 23, no. 1, pp. 123–144, 2004.

[2] S. de Jonge, C. van den Berg, R. J. de Vos, H. J. L. van der Heide, A. Weir, J. A. N. Verhaar, S. M. A. Bierma-Zeinstra, and J. L. Tol, "Incidence of midportion achilles tendinopathy in the general population," *British Journal of Sports Medicine*, vol. 45, no. 13, pp. 1026–1028, 2011. [Online]. Available: https://bjsm.bmj.com/content/45/13/1026

[3] A. Scott, K. Squier, H. Alfredson, R. Bahr, J. L. Cook, B. Coombes, R.-J. de Vos, S. N. Fu, A. Grimaldi, J. S. Lewis, N. Maffulli, S. Magnusson, P. Malliaras, S. Mc Auliffe, E. H. G. Oei, C. R. Purdam, J. D. Rees, E. K. Rio, K. Gravare Silbernagel, C. Speed, A. Weir, J. M. Wolf, I. v. d. Akker-Scheek, B. T. Vicenzino, and J. Zwerver, "Icon 2019: International scientific tendinopathy symposium consensus: Clinical terminology," *British Journal of Sports Medicine*, vol. 54, no. 5, pp. 260–262, 2020. [Online]. Available: https://bjsm.bmj.com/content/54/5/260

[4] R.-J. de Vos, A. C. Van Der Vlist, J. Zwerver, D. E. Meuffels, F. Smithuis, R. Van Ingen, F. Van Der Giesen, E. Visser, A. Balemans, M. Pols *et al.*, "Dutch multidisciplinary guideline on achilles tendinopathy," *British journal of sports medicine*, vol. 55, no. 20, pp. 1125–1134, 2021.

[5] M. Paavola, P. Kannus, T. A. Järvinen, K. Khan, L. Józsa, and M. Järvinen, "Achilles tendinopathy," *JBJS*, vol. 84, no. 11, pp. 2062–2076, 2002.

[6] P. Malliaras and S. O'Neill, "Potential risk factors leading to tendinopathy," *Apunts. Medicina de l'Esport*, vol. 52, no. 194, pp. 71–77, 2017.

[7] J. L. McCRORY, D. F. Martin, R. B. Lowery, D. W. Cannon, W. W. Curl, H. M. Read Jr, D. M. Hunter, T. Craven, and S. P. Messier, "Etiologic factors associated with achilles tendinitis in runners." *Medicine and science in sports and exercise*, vol. 31, no. 10, pp. 1374–1381, 1999.

[8] S. P. Magnusson, M. V. Narici, C. N. Maganaris, and M. Kjaer, "Human tendon behaviour and adaptation, in vivo," *The Journal of physiology*, vol. 586, no. 1, pp. 71–81, 2008.

[9] V. B. Shim, G. G. Handsfield, J. W. Fernandez, D. G. Lloyd, and T. F. Besier, "Combining in silico and in vitro experiments to characterize the role of fascicle twist in the achilles tendon," *Scientific Reports*, vol. 8, no. 1, p. 13856, 2018.

[10] J. Bojsen-Møller, P. Hansen, P. Aagaard, U. Svantesson, M. Kjaer, and S. P. Magnusson, "Differential displacement of the human soleus and medial gastrocnemius aponeuroses during isometric plantar flexor contractions in vivo," *Journal of applied physiology*, vol. 97, no. 5, pp. 1908–1914, 2004.

[11] C. Pizzolato, V. B. Shim, D. G. Lloyd, D. Devaprakash, S. J. Obst, R. Newsham-West, D. F. Graham, T. F. Besier, M. H. Zheng, and R. S. Barrett, "Targeted achilles tendon training and rehabilitation using personalized and real-time multiscale models of the neuromusculoskeletal system," *Frontiers in Bioengineering and Biotechnology*, p. 878, 2020.

[12] W. Hansen, V. B. Shim, S. Obst, D. G. Lloyd, R. Newsham-West, and R. S. Barrett, "Achilles tendon stress is more sensitive to subject-specific geometry than subject-specific material properties: a finite element analysis," *Journal of biomechanics*, vol. 56, pp. 26–31, 2017.

[13] T. J. MacGillivray, E. Ross, H. A. Simpson, and C. A. Greig, "3d freehand ultrasound for in vivo determination of human skeletal muscle volume," *Ultrasound in medicine & biology*, vol. 35, no. 6, pp. 928–935, 2009.

[14] L. Barber, R. Barrett, and G. Lichtwark, "Validation of a freehand 3d ultrasound system for morphological measures of the medial gastrocnemius muscle," *Journal of biomechanics*, vol. 42, no. 9, pp. 1313–1319, 2009.

[15] J. K. Sponbeck, C. R. Frandsen, S. T. Ridge, D. A. Swanson, D. C. Swanson, and A. W. Johnson, "Leg muscle cross-sectional area measured by ultrasound is highly correlated with mri," *Journal of Foot and Ankle Research*, vol. 14, pp. 1–7, 2021.

[16] G. M. Treece, R. W. Prager, A. H. Gee, and L. Berman, "Fast surface and volume estimation from non-parallel cross-sections, for freehand three-dimensional ultrasound," *Medical Image Analysis*, vol. 3, no. 2, pp. 141–173, 1999.

[17] S. J. Obst, R. Newsham-West, and R. S. Barrett, "In vivo measurement of human achilles tendon morphology using freehand 3-d ultrasound," *Ultrasound in medicine & biology*, vol. 40, no. 1, pp. 62–70, 2014.

[18] G. Weide, S. Van Der Zwaard, P. A. Huijing, R. T. Jaspers, and J. Harlaar, "3d ultrasound imaging: fast and cost-effective morphometry of musculoskeletal tissue," *JoVE (Journal of Visualized Experiments)*, no. 129, p. e55943, 2017.

[19] A. Fedorov, R. Beichel, J. Kalpathy-Cramer, J. Finet, J.-C. Fillion-Robin, S. Pujol, C. Bauer, D. Jennings, F. Fennessy, M. Sonka *et al.*, "3d slicer as an image computing platform for the quantitative imaging network," *Magnetic resonance imaging*, vol. 30, no. 9, pp. 1323–1341, 2012.

[20] S. Pieper, M. Halle, and R. Kikinis, "3d slicer," in *2004 2nd IEEE international symposium on biomedical imaging: nano to macro (IEEE Cat No. 04EX821)*. IEEE, 2004, pp. 632–635.

[21] R. Kikinis, S. D. Pieper, and K. G. Vosburgh, "3d slicer: a platform for subject-specific image analysis, visualization, and clinical support," in *Intraoperative imaging and image-guided therapy*. Springer, 2013, pp. 277–289.

[22] T. Illés and S. Somoskeöy, "The eos™ imaging system and its uses in daily orthopaedic practice," *International orthopaedics*, vol. 36, pp. 1325–1331, 2012.

[23] F. Fath, A. J. Blazevich, C. M. Waugh, S. C. Miller, and T. Korff, "Direct comparison of in vivo achilles tendon moment arms obtained from ultrasound and mr scans," *Journal of applied physiology*, vol. 109, no. 6, pp. 1644–1652, 2010.

[24] V. B. Shim, W. Hansen, R. Newsham-West, L. Nuri, S. Obst, C. Pizzolato, D. G. Lloyd, and R. S. Barrett, "Influence of altered geometry and material properties on tissue stress distribution under load in tendinopathic achilles tendons–a subject-specific finite element analysis," *Journal of Biomechanics*, vol. 82, pp. 142–148, 2019.

[25] J. A. Weiss, B. N. Maker, and S. Govindjee, "Finite element implementation of incompressible, transversely isotropic hyperelasticity," *Computer methods in applied mechanics and engineering*, vol. 135, no. 1-2, pp. 107–128, 1996.

[26] G. A. Holzapfel, T. C. Gasser, and R. W. Ogden, "A new constitutive framework for arterial wall mechanics and a comparative study of material models," *Journal of elasticity and the physical science of solids*, vol. 61, pp. 1–48, 2000.

[27] P. Diniz, C. Quental, P. Violindo, J. Veiga Gomes, H. Pereira, G. M. Kerkhoffs, F. C. Ferreira, and J. Folgado, "Design and validation of a finite element model of the aponeurotic and free achilles tendon," *Journal of Orthopaedic Research®*, vol. 41, no. 3, pp. 534–545, 2023.

[28] V. B. Shim, J. W. Fernandez, P. B. Gamage, C. Regnery, D. W. Smith, B. S. Gardiner, D. G. Lloyd, and T. F. Besier, "Subject-specific finite element analysis to characterize the influence of geometry and material properties in achilles tendon rupture," *Journal of biomechanics*, vol. 47, no. 15, pp. 3598–3604, 2014.

[29] T. C. Gasser, R. W. Ogden, and G. A. Holzapfel, "Hyperelastic modelling of arterial layers with distributed collagen fibre orientations," *Journal of the royal society interface*, vol. 3, no. 6, pp. 15–35, 2006.

[30] C. C. van Gils, R. H. Steed, and J. C. Page, "Torsion of the human achilles tendon," *The Journal of foot and ankle surgery*, vol. 35, no. 1, pp. 41–48, 1996.

[31] T. Fukunaga, R. Roy, F. Shellock, J. Hodgson, M. Day, P. Lee, H. Kwong-Fu, and V. Edgerton, "Physiological cross-sectional area of human leg muscles based on magnetic resonance imaging," *Journal of orthopaedic research*, vol. 10, no. 6, pp. 926–934, 1992.

[32] L. Stenroth, D. Thelen, and J. Franz, "Biplanar ultrasound investigation of in vivo achilles tendon displacement non-uniformity," *Translational sports medicine*, vol. 2, no. 2, pp. 73–81, 2019.

[33] G. G. Handsfield, J. Greiner, J. Madl, E. A. Rog-Zielinska, E. Hollville, B. Vanwanseele, and V. Shim, "Achilles subtendon structure and behavior as evidenced from tendon imaging and computational modeling," *Frontiers in Sports and Active Living*, vol. 2, p. 70, 2020.

[34] S. Wolfram, E. F. Hodson-Tole, C. I. Morse, K. L. Winwood, and I. M. McEwan, "Elongation differences between the sub-tendons of gastrocnemius medialis and lateralis during plantarflexion in different frontal plane position of the foot," *Gait & Posture*, vol. 75, pp. 149–154, 2020.

[35] W. H. Clark and J. R. Franz, "Do triceps surae muscle dynamics govern non-uniform achilles tendon deformations?" *PeerJ*, vol. 6, p. e5182, 2018.

[36] P. Szaro, W. Cifuentes Ramirez, S. Borkmann, A. Bengtsson, M. Polaczek, and B. Ciszek, "Distribution of the subtendons in the midportion of the achilles tendon revealed in vivo on mri," *Scientific Reports*, vol. 10, no. 1, p. 16348, 2020.

[37] K. Albracht, A. Arampatzis, and V. Baltzopoulos, "Assessment of muscle volume and physiological cross-sectional area of the human triceps surae muscle in vivo," *Journal of biomechanics*, vol. 41, no. 10, pp. 2211–2218, 2008.

[38] H. Haxton, "Absolute muscle force in the ankle flexors of man," *The Journal of physiology*, vol. 103, no. 3, p. 267, 1944.

[39] T. M. Grant, L. E. Diamond, C. Pizzolato, B. A. Killen, D. Devaprakash, L. Kelly, J. N. Maharaj, and D. J. Saxby, "Development and validation of statistical shape models of the primary functional bone segments of the foot," *PeerJ*, vol. 8, p. e8397, 2020.

[40] G. Davico, C. Pizzolato, B. A. Killen, M. Barzan, E. K. Suwarganda, D. G. Lloyd, and C. P. Carty, "Best methods and data to reconstruct paediatric lower limb bones for musculoskeletal modelling," *Biomechanics and Modeling in Mechanobiology*, vol. 19, pp. 1225–1238, 2020.

[41] H. X. Hoang, C. Pizzolato, L. E. Diamond, and D. G. Lloyd, "Subject-specific calibration of neuromuscular parameters enables neuromusculoskeletal models to estimate physiologically plausible hip joint contact forces in healthy adults," *Journal of biomechanics*, vol. 80, pp. 111–120, 2018.

[42] A. Arndt, A.-S. Bengtsson, M. Peolsson, A. Thorstensson, and T. Movin, "Non-uniform displacement within the achilles tendon during passive ankle joint motion," *Knee Surgery, Sports Traumatology, Arthroscopy*, vol. 20, pp. 1868–1874, 2012.

[43] S. Bogaerts, C. De Brito Carvalho, L. Scheys, K. Desloovere, J. D'hooge, F. Maes, P. Suetens, and K. Peers, "Evaluation of tissue displacement and regional strain in the achilles tendon using quantitative high-frequency ultrasound," *PloS one*, vol. 12, no. 7, p. e0181364, 2017.

[44] I. Sancho, P. Malliaras, C. Barton, R. W. Willy, and D. Morrissey, "Biomechanical alterations in individuals with achilles tendinopathy during running and hopping: A systematic review with meta-analysis," *Gait & posture*, vol. 73, pp. 189–201, 2019.
[45] M. Ekiert, K. A. Tomaszewski, and A. Mlyniec, "The differences in viscoelastic properties of subtendons result from the anatomical tripartite structure of human achilles tendon-ex vivo experimental study and modeling," *Acta biomaterialia*, vol. 125, pp. 138–153, 2021.
[46] L. C. Slane, J. Martin, R. DeWall, D. Thelen, and K. Lee, "Quantitative ultrasound mapping of regional variations in shear wave speeds of the aging achilles tendon," *European radiology*, vol. 27, pp. 474–482, 2017.
[47] S. Aubry, J.-R. Risson, A. Kastler, B. Barbier-Brion, G. Siliman, M. Runge, and B. Kastler, "Biomechanical properties of the calcaneal tendon in vivo assessed by transient shear wave elastography," *Skeletal radiology*, vol. 42, pp. 1143–1150, 2013.
[48] R. J. DeWall, L. C. Slane, K. S. Lee, and D. G. Thelen, "Spatial variations in achilles tendon shear wave speed," *Journal of biomechanics*, vol. 47, no. 11, pp. 2685–2692, 2014.
[49] C. Payne, P. Watt, M. Cercignani, and N. Webborn, "Reproducibility of shear wave elastography measuresof the achilles tendon," *Skeletal Radiology*, vol. 47, pp. 779–784, 2018.
[50] X.-M. Chen, L.-G. Cui, P. He, W.-W. Shen, Y.-J. Qian, and J.-R. Wang, "Shear wave elastographic characterization of normal and torn achilles tendons: a pilot study," *Journal of ultrasound in Medicine*, vol. 32, no. 3, pp. 449–455, 2013.
[51] P. Corrigan, J. A. Zellers, P. Balascio, K. G. Silbernagel, and D. H. Cortes, "Quantification of mechanical properties in healthy achilles tendon using continuous shear wave elastography: a reliability and validation study," *Ultrasound in medicine & biology*, vol. 45, no. 7, pp. 1574–1585, 2019.
[52] R. J. Cunningham, P. J. Harding, and I. D. Loram, "Real-time ultrasound segmentation, analysis and visualisation of deep cervical muscle structure," *IEEE transactions on medical imaging*, vol. 36, no. 2, pp. 653–665, 2016.
[53] D. R. Nolan, A. L. Gower, M. Destrade, R. W. Ogden, and J. McGarry, "A robust anisotropic hyperelastic formulation for the modelling of soft tissue," *Journal of the mechanical behavior of biomedical materials*, vol. 39, pp. 48–60, 2014.
[54] J. Peltonen, N. J. Cronin, L. Stenroth, T. Finni, and J. Avela, "Viscoelastic properties of the achilles tendon in vivo," *Springerplus*, vol. 2, no. 1, pp. 1–8, 2013.
[55] M. Ekiert, K. A. Tomaszewski, and A. Mlyniec, "The differences in viscoelastic properties of subtendons result from the anatomical tripartite structure of human achilles tendon-ex vivo experimental study and modeling," *Acta Biomaterialia*, vol. 125, pp. 138–153, 2021.
[56] H. Khayyeri, G. Longo, A. Gustafsson, and H. Isaksson, "Comparison of structural anisotropic soft tissue models for simulating achilles tendon tensile behaviour," *Journal of the mechanical behavior of biomedical materials*, vol. 61, pp. 431–443, 2016.
[57] J. A. Kadlowec, S. P. Lake, K. S. Miller, L. J. Soslowsky, and D. M. Elliott, "Modeling of human supraspinatus tendon using a hyperelastic model with distributed fiber orientations," in *ASME Summer Bioengineering Conference*, 2009, pp. 17–21.
[58] ——, "A hyperelastic model with distributed fibers to describe human supraspinatus tendon tensile mechanics," in *Summer Bioengineering Conference*, vol. 48913. American Society of Mechanical Engineers, 2009, pp. 679–680.
[59] M. Edama, M. Kubo, H. Onishi, T. Takabayashi, T. Inai, E. Yokoyama, W. Hiroshi, N. Satoshi, and I. Kageyama, "The twisted structure of the human a chilles tendon," *Scandinavian journal of medicine & science in sports*, vol. 25, no. 5, pp. e497–e503, 2015.

APPENDIX

A. *Stress-Strain Analysis Cylinder Geometry*

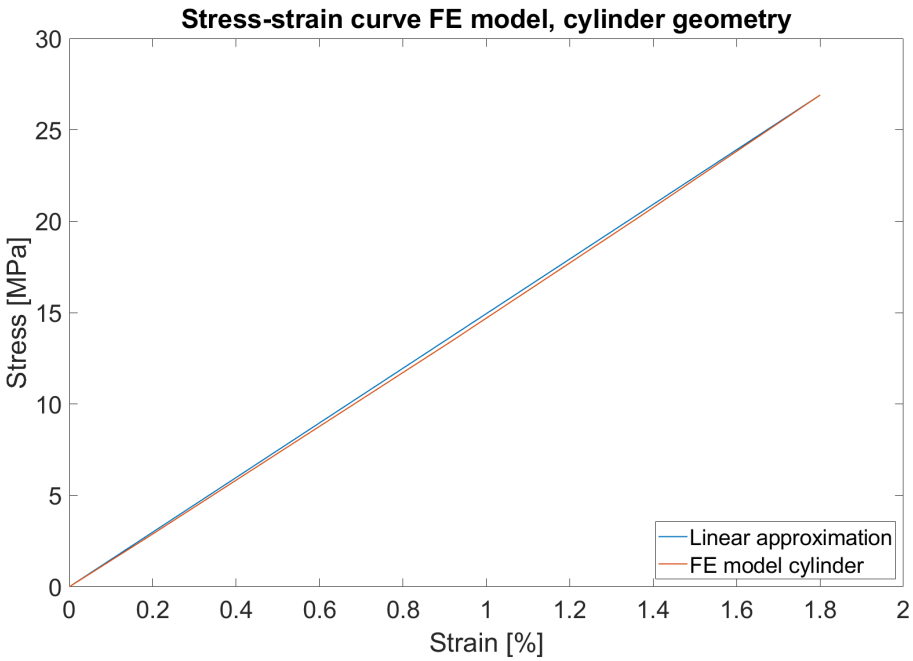

Fig. 12: Stress-strain curve of the Neo-Hookean model combined with the Holzapfel-Gasser-Ogden model applied on a cylinder geometry, using parameters and maximum force as used in the Achilles tendon model. A linear approximation, based on the first and last point of the curve, was plotted for linearity testing.